

Radiation-Defect Resistance in Optimally Doped $\text{La}_{2-x}\text{Sr}_x\text{CuO}_4$: Constraints on Models of Electrical Transport

J. A. Clayhold¹, O. Pelleg², D. C. Ingram³, A. T. Bollinger², G. Logvenov², D. W. Rench¹, B. M. Kerns¹, M. D. Schroer¹, R. J. Sundling⁴ and I. Bozovic²

¹*Department of Physics, Miami University, Oxford, Ohio 45056, USA*

²*Brookhaven National Laboratory, Upton, New York 11973-5000, USA*

³*Department of Physics and Astronomy, Ohio University, Athens, Ohio 45701, USA*

⁴*ZenSoft Inc., Madison, WI 53705*

Abstract

Precise measurements are reported of the temperature dependence of additional resistivity caused by scattering on columnar defects created in $\text{La}_{1.84}\text{Sr}_{0.16}\text{CuO}_4$ by heavy-ion irradiation, and the results are used to constrain the models of carrier transport. Previous magneto-transport studies have delineated two distinct scattering processes, proportional to T and T^2 , respectively. Our new radiation-defect scattering results suggest strongly that the two processes act as parallel conduction channels.

Unraveling the mystery of high-temperature superconductivity (HTS) is one of the most important open problems in condensed matter physics. Many believe that a necessary first step is to fully understand the normal state from which HTS emerges, in particular its peculiar transport properties. However, this is still a matter of substantial controversy. In particular, it has been debated whether the proper description should be based on one or multi-component models. [1] The first broad class includes some of the most popular HTS models including the single-band two-dimensional Hubbard model and the so-called t - J model. [2-5] It is supported by Angle-resolved photoelectron spectroscopy (ARPES) and scanning tunneling microscopy (STM) measurements, which have been the primary source of information about the electronic states in cuprates. [6-9] In optimally doped and overdoped cuprates with a single CuO_2 layer, such as $\text{La}_{2-x}\text{Sr}_x\text{CuO}_4$ (LSCO), both ARPES and STM reveal only one large Fermi surface, indicative of a degenerate ($kT \ll E_F$) gas of charge carriers (holes). While it is of some concern that both techniques are very surface-sensitive, recent angle-dependent magneto-resistance oscillations (AMRO) measurements, which probe the bulk, on overdoped (OD) cuprate superconductors have provided Fermi surfaces that agree quantitatively with those derived by ARPES. [10,11] Transport in OD cuprates is dominated by a relaxation rate proportional to the square of the absolute temperature, T^2 . As the doping level and the hole density are reduced, this slowly gives way to scattering linear in T . [10] Interestingly, the appearance of the T -linear scattering is correlated with the occurrence of superconductivity at lower temperatures. [11] In the highly-overdoped materials, which are more metallic than optimally-doped (OP) materials, AMRO measurements revealed which portions of Fermi surface contribute to the T -linear and T -quadratic carrier relaxation processes: the T^2 scattering appears everywhere while the T -linear scattering is predominantly associated with momentum directions parallel to the copper-oxygen bonds. [10]

On the other hand, a number of experimental findings support the two-component scenario. As the temperature and/or the doping level are tuned, both the Hall effect and the thermo-power have been observed to change sign, possibly indicating coexistence of both hole and electron pockets. [12,13] More conclusively, recent observations of quantum (de Haas-van Alphen and Shubnikov-de Haas) oscillations clearly reveal existence of two or even three pockets. [14-19] Some of these are small and suggestive of non-degenerate ($kT > E_F$) carriers with a large effective mass. The latter is also consistent with earlier experimental and theoretical studies of Nuclear magnetic resonance (NMR). [20-22]

The most discerning magneto-transport probes, including AMRO measurements, are not easily applied to the most interesting, OP cuprates. At optimal doping, transport is strongly dominated by the momenta along the nodal directions, and yet the resistance appears to have both linear-T and quadratic-T contributions. [23] But from the resistivity alone it has not been possible to decide whether at optimal doping the two forms of scattering, T and T^2 , act as parallel conductance channels or as additive scattering rates.

In the work reported here, we make use of a largely overlooked but powerful resource - measuring the temperature dependence of the defect-scattering resistance. When different Fermi surface pockets or regions contribute to conduction with different temperature dependences, then the gradual degradation of each contribution via added scattering alters the balance between the two in a characteristic way that reveals much about how transport varies around the Fermi surface. Impurity resistance measurements offer much of the same information available from conventional magneto-transport measurements such as the Hall effect but with the advantage that they are less complicated to model and interpret.

However, some care is necessary with such measurements, because in $\text{La}_{1.84}\text{Sr}_{0.16}\text{CuO}_4$ the impurity resistance varies by only 15% between 50 K and room temperature, so it is desired to control and measure the defect-scattering resistance to better than 1%. A particularly good method for controlling defect scattering is the progressive radiation damage of high-quality thin film samples. [24]. Point defects from electron-beam or proton irradiation are known to self-anneal even at very low temperatures. [25] Columnar damage tracks caused by high-energy (1 MeV) ions are less susceptible to self-annealing effects. [26] Hence, for this study we have developed a method in which a single LSCO film is exposed to irradiation by high-energy ions with a large gradient of dose, and thus in the induced defect density, across the wafer. This is followed by a 4-point-contact resistance measurement of 30 different lithographically defined samples (pixels). While each pixel is exposed to a different and known ion irradiation dose, all the pixels are measured simultaneously during a single cool-down so that all of them share the same thermal history. This should alleviate the problem of self-annealing; indeed, we have observed no time-dependence and aging effects.

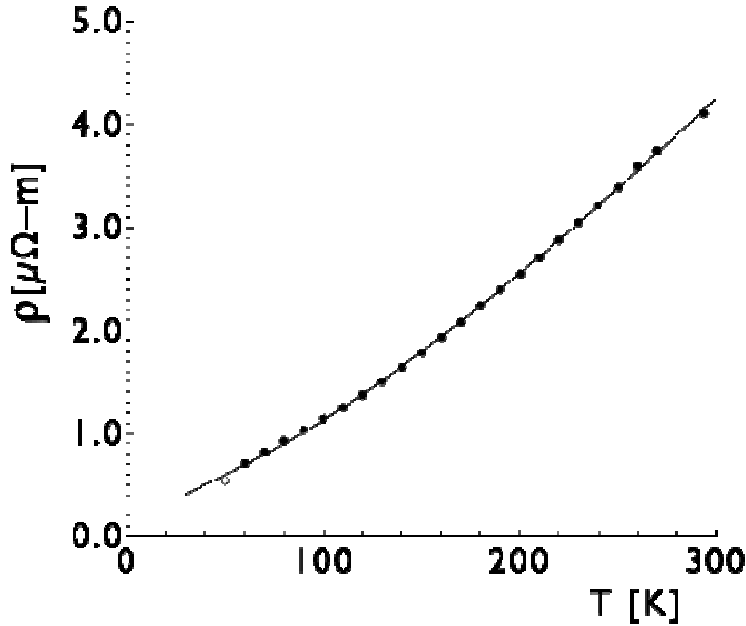


Fig. 1: Resistivity of a 480 nm thick film of $\text{La}_{1.84}\text{Sr}_{0.16}\text{CuO}_4$ grown by atomic layer-by-layer molecular beam epitaxy (ALL-MBE). The curve fit was performed simultaneously with the data of Fig. 3, and it includes contributions from scattering rates linear and quadratic in T , as well as a small contribution from residual defect scattering.

A highly-uniform single-crystal film of $\text{La}_{1.84}\text{Sr}_{0.16}\text{CuO}_4$ was grown on a LaSrAlO_4 substrate that had been polished with the surface perpendicular to the (001) crystallographic direction. The film was grown in a unique atomic layer-by-layer molecular beam epitaxy (ALL-MBE) system [27] devoted to the synthesis of atomically-precise [28,29] oxide films. During film growth, both the layer-by-layer epitaxy and the instantaneous stoichiometry are monitored in real time using multiple advanced characterization tools, including Reflection high energy electron diffraction (RHEED) and Time-of-flight ion scattering and recoil spectroscopy (TOF-ISARS). Gold contacts were made in-situ without breaking vacuum. The film was patterned using optical photoresist and a combination of ion milling and chemical etching. More details of the system design, film growth and patterning have been previously described. [27]

For electrical transport measurements we used a specially constructed system capable of simultaneous measurement of the both resistance and the Hall effect at 30 locations on a single film, as a function of temperature. [30] We characterized the as-grown film of $\text{La}_{1.84}\text{Sr}_{0.16}\text{CuO}_4$ prior to irradiation. The sample was highly uniform, with the exception of a few pixels near the edge of the wafer which may have experienced a different post-growth cooling rate and consequent small changes of local oxygen content. Excluding those few channels, statistical analysis of the multi-channel resistance data indicated that the channel-to-channel variation of the resistance caused by defect scattering was only 0.086Ω , accounting for 0.01% of the room temperature resistance of 85Ω . [31] The effect of lithographic patterning variations on the measured transport properties was measured to be less than 0.05%. [31] The largest contribution to channel-to-channel changes in electrical transport was determined to come from small fluctuations of total stoichiometry — most likely the oxygen content — but still amounting to just 0.41% of the total sample resistance. [31] By contrast, the subsequent ion-induced damage increased the room temperature

resistance by 10% and the resistance at 50 K by 80%, dwarfing the random channel-to-channel variation in the as-grown film.

Ion irradiation was performed at the W. M. Keck Thin Film Analysis Facility, using the 4.5 MeV tandem accelerator in the Edwards Accelerator Laboratory at Ohio University. For oxygen ions at an incident energy of 1 MeV, numerical calculations [32] indicate that the main effect on the 480 nm thick film of $\text{La}_{1.84}\text{Sr}_{0.16}\text{CuO}_4$ should be columnar damage tracks. The energy was chosen for a stopping range much longer than the film thickness, so that the largest part of the incident energy — with the attendant possibility of local amorphization — is deposited deep in the substrate below the film. The beam was slightly defocused and then raster-scanned under computer control to achieve a smooth gradient of the fluence, ranging from zero at one edge of the film to $5 \times 10^{13} \text{ cm}^{-2}$ at the opposite edge.

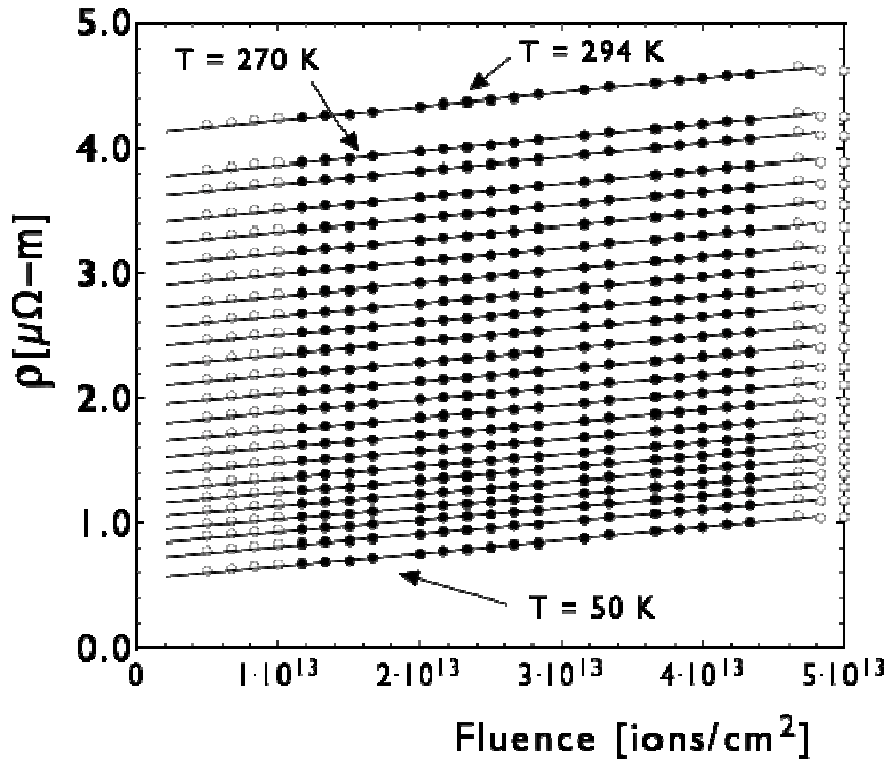


Fig. 2: Resistivity of the 480 nm thick film of $\text{La}_{1.84}\text{Sr}_{0.16}\text{CuO}_4$ film as a function of the fluence of 1 MeV oxygen ions, measured at 24 different temperatures between 50 K and 294 K. Measurement channels at the film edges (corresponding to the highest and the lowest fluences) were not used for fitting the dependence of ρ on the fluence F , because of small stoichiometry deviations. A small number of gaps occur for measurement channels whose electrical contacts failed upon cool down. The solid line is the best linear fit for $d\rho/dF$.

The effects of the ion irradiation on the measured resistance are shown in Fig. 2 where each curve represents a different temperature with data taken at 10 K intervals. Each discrete point on the horizontal axis represents a different fluence, measured at a different location (pixel) on the film. With the exception of a few locations at the edges of the film as previously discussed, and a few locations for which the electrical contacts failed during cool down, the additional resistance caused by the ion damage shows excellent linearity with total ion dose. The high linearity of ad-

ditional resistance suggests strongly that the induced damage is neither trapping holes nor doping additional carriers. The solid points in Fig. 2 were used for linear fits to determine the derivative dp/dF of the resistivity with respect to the fluence. The temperature dependence of dp/dF is shown in Fig. 3.

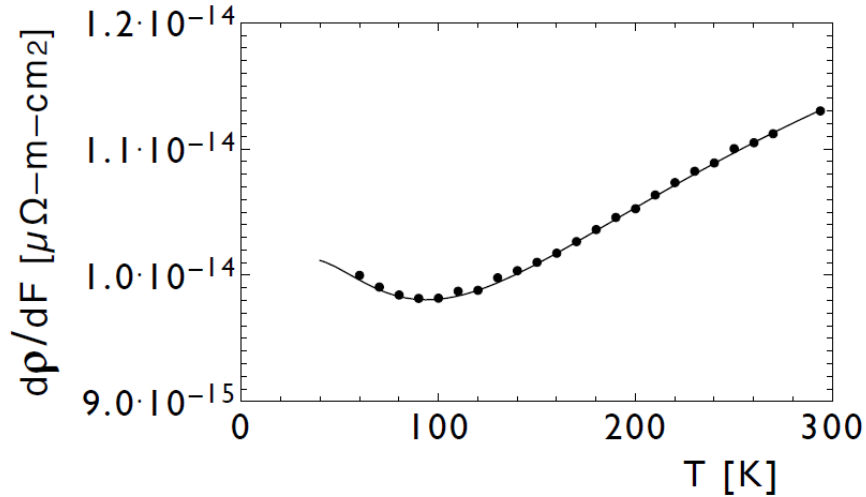


Fig. 3: Slopes of the linear fits to the data of Fig. 2, showing the temperature dependence of the extra resistance caused by ion damage. The solid line is a curve fit to Eqs. 3, 5, and 6, performed simultaneously with the data of Fig. 1.

From the Boltzmann equation without a magnetic field, the electric conductivity tensor,

$$\sigma = \frac{e^2}{4\pi^3\hbar} \int \vec{\ell}_k d\vec{\mathcal{S}} \quad (1)$$

[33] is an integral of the direct tensor product of the mean free path vector l and the normal to a patch of Fermi surface dS . The Fermi surface is parameterized as $k_F(\phi)$, where k_F is the Fermi wavevector and ϕ is the angle from the x-direction, $(0, \pi)$. When the Fermi surface is not circular, the angle γ between the Fermi wavevector and the unit normal to the Fermi surface is non-zero. The longitudinal conductivity σ_{xx} is obtained from Eq. 1 by projecting each vector l and dS onto the x-axis, yielding a factor of $\cos^2(\phi)$ for a circular Fermi surface, or $\cos^2(\phi - \gamma)$ for a non-circular Fermi surface. [34] The area of the differential patch dS of a circular Fermi surface is $(2\pi/c_0)k_F d\phi$ where c_0 is the z-axis lattice constant. When the Fermi surface is not circular, dS acquires an additional geometric factor of $1/\cos(\gamma)$. [34] The longitudinal electric conductivity is conveniently written as $\sigma = \int L(\phi) W(\phi) d\phi$, where $L(\phi)$ is **XXXX** and the angular weight factor $W(\phi)$ depends only on constants and static properties of the Fermi surface. [35]

$$W(\phi) = \frac{e^2}{4\pi^3\hbar} \left(\frac{2\pi}{c_0} \right) \frac{k_F \cos^2(\phi - \gamma)}{\cos \gamma} \quad (2)$$

By fitting the hopping integrals and Fermi energies to a series of measured Fermi surfaces [36] for LSCO, we can interpolate a Fermi surface for $\text{La}_{1.84}\text{Sr}_{0.16}\text{CuO}_4$, and then compute the total angular weight $W_0 = \int W(\phi) d\phi = 0.0413 (\mu\Omega\text{-m-}\text{\AA})^{-1}$

Upon irradiation, induced defects from a total ion fluence F shorten the mean free path of the pristine material: $L_0^{-1} + FD$, where D is the average scattering cross-section, taken as an effective diameter of the columnar damage tracks. The additivity of inverse mean free paths leads to the important result that $dL/dF = -DL^2$ at all values of F . The derivative of the longitudinal conductivity with respect to fluence is $d\sigma/dF = -D \int L^2(\phi) W(\phi) d\phi$. Inverting the conductivity to find the effect of ion damage on the resistivity yields

$$\frac{d\rho}{dF} = \frac{D \int \ell^2(\phi) W(\phi) d\phi}{[\int \ell(\phi) W(\phi) d\phi]^2} \quad (3)$$

The temperature dependence of the impurity resistance $d\rho/dF$ enters through the temperature-dependent mean free path $L(\phi) = L(\phi, T)$. It is apparent from Eq. 3 that the impurity resistivity becomes independent of the temperature whenever one part of the Fermi surface dominates the electrical transport or if there is a common temperature dependence of the mean free path at all places on the Fermi surface. In $\text{La}_{1.84}\text{Sr}_{0.16}\text{CuO}_4$ we observe a 15% variation of $d\rho/dF$ between $T = 50$ K and $T = 294$ K. Accommodating that 15% variation has provided strong constraints on the distribution of different carrier relaxation processes.

To fit the data, we adopt a two-component transport model in which the conductivity has dominant contributions from two different conductance channels as might originate from different Fermi surface pockets or patches (labeled ‘a’ and ‘b’):

$$\sigma_{xx}(T) = W_a^{xx} \ell_a(T) + W_b^{xx} \ell_b(T) \quad (4)$$

where the two weight factors satisfy $W_a + W_b = W_0$, i.e., $W_a = f_W W_0$ and $W_b = (1 - f_W) W_0$ with f_W between 0 and 1. It should be noted that, although the form of Eq. 4 derives from a model of conductivity from different pockets or patches of Fermi surface, it can also be interpreted as the summed contributions from any two conduction processes, which might even occur at the same point on Fermi surface.

We use general forms for the two mean free paths in Eq. 4:

$$\begin{aligned} \ell_a(T) &= \frac{1}{a_0 + a_1 T + a_2 T^2} \\ \ell_b(T) &= \frac{1}{b_0 + b_1 T + b_2 T^2} \end{aligned} \quad (5a) \text{ and } (5b)$$

such that each of the two mean free paths can provide for a combination of constant, T-linear or T-squared resistivity. This choice is sufficiently general to provide for both a series combination of linear and quadratic resistivity, as well as a parallel combination. Together, the temperature coefficients ($a_0, a_1, a_2, b_0, b_1, b_2$) as well as the weight partitioning factor f_w and the effective diameter D , are used for simultaneous curve fits to both the measured resistivity data and the impurity resistance data $d\rho/dF$. We find that the simultaneous curve fits to the data of Figs. 1 and 3 appear to be robust by current analytical methods; in particular, two of the free parameters (a_2 and b_1 ; or, by symmetry, b_2 and a_1) are always driven to zero by the fitting process. The parallel resistor model appears to describe accurately transport in LSCO near optimal doping. Our main result is that the linear and the quadratic contributions to the resistivity of $\text{La}_{1.84}\text{Sr}_{0.16}\text{CuO}_4$ combine as additive conductances.

a_0 [\AA^{-1}]	a_1 [$\text{\AA}^{-1}\text{K}^{-1}$]	b_0 [\AA^{-1}]	b_2 [$\text{\AA}^{-1}\text{K}^{-2}$]	f_w	D [\AA]
8.728×10^{-3}	4.217×10^{-4}	1.113×10^{-2}	4.215×10^{-6}	0.662	4.050

TABLE I: Final fitting parameters to the temperature-dependent resistivity $\rho(T)$ and impurity resistivity $d\rho(T)/dF$.

The best fit results are shown in Table I. Parameters that returned a best fit value of zero are not listed. The resulting curve fits are shown in Figs. 1 and 3. The effective value of the diameter of the columnar damage tracks D is found to be 4.09 \AA , comparable to the a -axis parameter of 3.77 \AA in our epitaxial films. The T-linear scattering rate implicit in the value of the parameter a_1 , taken by itself, would correspond to a mean free path of 24 \AA at $T=100 \text{ K}$. The quadratic scattering rate implicit in the value of b_2 , taken by itself, would correspond to a mean free path of 33 \AA at $T=100 \text{ K}$. These absolute mean free paths are only estimates because in their normalization we assumed that the entire Fermi surface of $\text{La}_{1.84}\text{Sr}_{0.16}\text{CuO}_4$ contributes to the measured transport results, which need not be the case.

To conclude, we find that the temperature dependence of the radiation-defect-scattering resistance, as described by Eq. 3, allows for a simple and robust analysis of the distribution of transport mean free paths around the Fermi surface. For the case of optimally-doped LSCO, the data and the analysis indicate that both T-linear and T-quadratic relaxation channels contribute to the resistance as parallel (additive) conduction processes, which may occur at distinct portions or pockets of the Fermi surface.

References

- [1] D. N. Basov and T. Timusk, *Rev. Mod. Phys.* **77**, 721-779 (2005).
- [2] F. C. Zhang and T. M. Rice, *Phys. Rev. B* **37**, 3759-3761 (1988).
- [3] E. Manousakis, *Rev. Mod. Phys.* **63**, 1-62 (1991).
- [4] E. Dagotto, *Rev. Mod. Phys.* **66**, 763-840 (1994).
- [5] P. A. Lee, N. Nagaosa and X. G. Wen, *Rev. Mod. Phys.* **78**, 17-85 (2006).
- [6] A. Ino, C. Kim, M. Nakamura M, et al. *Phys. Rev. B* **65**, 094504 (2002).
- [7] A. Damascelli, Z. Hussain and Z.-X. Shen, *Rev. Mod. Phys.* **75**, 473-541 (2003).
- [8] J. E. Hoffman, K. McElroy, D. H. Lee, K. M. Lang, H. Eisaki, S. Uchida, and J. C. Davis, *Science*, **297**, 1148-1151 (2002).
- [9] K. McElroy, R. W. Simmonds, J. E. Hoffman, D. H. Lee, J. Orenstein, H. Eisaki, S. Uchida, and J. C. Davis, *Nature* **422**, 592-596 (2003).
- [10] M. Abdel-Jawad, M. Kennett, L. Balicas, A. Carrington, A. Mackenzie, R. McKenzie, and N. E. Hussey, *Nature Physics* **2**, 821 (2006).
- [11] M. Abdel-Jawad, J. G. Analytis, L. Balicas, A. Carrington, J. P. H. Charmant, M. M. J. French, and N. E. Hussey, *Phys. Rev. Lett.* **99**, 107002 (2007).
- [12] D. LeBoeuf, N. Doiron-Leyraud, J. Levallois, R. Daou, J. B. Bonnemaïson, N. E. Hussey, L. Balicas, B. J. Ramshaw, R. X. Liang, D. A. Bonn, W. N. Hardy, S. Adachi, C. Proust, and L. Taillefer, *Nature* **450**, 533-536 (2007).
- [13] D. D. Obertelli, J. R. Cooper and J. L. Tallon, *Phys. Rev. B* **46**, 14928-14931 (1992).
- [14] N. Doiron-Leyraud, C. Proust, D. LeBoeuf, J. Levallois, J. B. Bonnemaïson, R. X. Liang, D. A. Bonn, W. N. Hardy, and L. Taillefer, *Nature* **447**, 565-568 (2007).
- [15] E. A. Yelland, J. Singleton, C. H. Mielke, N. Harrison, F. F. Balakirev, B. Dabrowski and J. R. Cooper, *Phys. Rev. Lett.* **100**, 047003 (2008).
- [16] A. F. Bangura, J. D. Fletcher, A. Carrington, J. Levallois, M. Nardone, B. Vignolle, P. J. Heard, N. Doiron-Leyraud, D. LeBoeuf, L. Taillefer, S. Adachi, C. Proust, and N. E. Hussey, *Phys. Rev. Lett.* **100**, 047004 (2008).
- [17] C. Jaudet, D. Vignolles, A. Adouard, J. Levallois, D. LeBoeuf, N. Doiron-Leyraud, B. Vignolle, M. Nardone, A. Zitouni, R. X. Liang, D. A. Bonn, W. N. Hardy, L. Taillefer, and C. Proust, *Phys. Rev. Lett.* **100**, 187005 (2008).

- [18] S. E. Sebastian, N. Harrison, E. Palm, T. P. Murphy, C. H. Mielke, R. X. Liang, D. A. Bonn, W. N. Hardy, and G. G. Lonzarich, *Nature*, **454**, 200-203 (2008).
- [19] B. Vignolle, A. Carrington, R. A. Cooper, M. M. J. French, A. P. Mackenzie, C. Jaudet, D. Vignolles, C. Proust, and N. E. Hussey, *Nature*, **455**, 952-955 (2008).
- [20] T. Machi, I. Tomeno, T. Miyatake, N. Koshizuka, S. Tanaka, T. Imai and H. Yasuoka, *Physica C* **173**, 32-36 (1991).
- [21] A. S. Alexandrov, *J. Low. Temp. Phys.* **87**, 721-729 (1992).
- [22] A. S. Alexandrov and N. F. Mott, *Rept. Prog. Phys.* **57**, 1197-1288 (1994).
- [23] R. A. Cooper, Y. Wang, B. Vignolle, O. J. Lipscombe, S. M. Hayden, Y. Tanabe, T. Adachi, Y. Koike, M. Nohara, H. Takagi, C. Proust, and N. E. Hussey, *Science* **323**, 603 (2009).
- [24] J. Ziegler and T. Cahill, *New uses of ion accelerators* (Plenum Press New York, 1975).
- [25] A. Hughes and D. Pooley, *Real solids and radiation* (Taylor & Francis, 1975).
- [26] A. M. Petrean, L. M. Paulius, Y. Yan, M. A. Kirk, W.-K. Kwok, and G. W. Crabtree, *Phys. Rev. B* **64**, 134527 (2001).
- [27] I. Bozovic, *IEEE Trans. Appl. Supercon.* **11**, 2686 (2001).
- [28] I. Bozovic, G. Logvenov, M. Verhoeven, P. Caputo, E. Goldobin, and T. Geballe, *Nature* **422**, 873 (2003).
- [29] I. Bozovic, G. Logvenov, M. Verhoeven, P. Caputo, E. Goldobin, and M. Beasley, *Phys. Rev. Lett.* **93**, 157002 (2004).
- [28] J. Clayhold, B. Kerns, M. Schroer, D. Rench, G. Logvenov, A. Bollinger, and I. Bozovic, *Rev. Sci. Instrum.* **79**, 033908 (2008).
- [29] J. Clayhold, O. Pelleg, A. Bollinger, G. Logvenov, B. Kerns, M. Schroer, D. Rench, and I. Bozovic, *J. Supercond. Nov. Magn.* (2009) to appear.
- [30] J. Ziegler, J. Biersack, and M. Ziegler, *SRIM - The stopping and range of ions in matter* (SRIM Co., 2008).
- [31] J. Ziman, *Electrons and phonons* (Oxford University Press New York, 2001).
- [32] N. Hussey, *Eur. Phys. J. B* **31**, 495 (2003).

- [33] c.f. appendix to Ref. 32.
- [34] T. Yoshida, X. J. Zhou, K. Tanaka, W. L. Yang, Z. Hussain, Z.-X. Shen, A. Fujimori, S. Sahrakorpi, M. Lindroos, R. S. Markiewicz, A. Bansil, S. Komiya, Y. Ando, H. Eisaki, T. Kakeshita, and S. Uchida, *Phys. Rev. B* **74**, 224510 (2006).
- [35] N. P. Ong, *Phys. Rev. B* 43, 193 (1991).